Disentangling the mechanisms of ENSO response to tropical volcanic eruptions

Francesco S.R. Pausata[1], Yang Zhao[2], Davide Zanchettin[3], Rodrigo Caballero[4], and David S. Battisti[5]

[1]University of Quebec in Montreal
[2]Chinese Academy of Meteorological Sciences
[3]University Ca'Foscari of Venice
[4]Stockholm University
[5]University of Washington

November 22, 2022

Abstract

Stratospheric volcanic aerosol can have major impacts on global climate. Despite a consensus among studies on an El Niño–like response in the first or second post-eruption year, the mechanisms that trigger a change in the state of El Niño-Southern Oscillation (ENSO) following volcanic eruptions are still debated. Here, we shed light on the processes that govern the ENSO response to tropical volcanic eruptions through a series of sensitivity experiments with an Earth System Model where a uniform stratospheric volcanic aerosol loading is imposed over different parts of the tropics. Three tropical mechanisms are tested: the "ocean dynamical thermostat" (ODT); the cooling of the Maritime Continent; and the cooling of tropical northern Africa (NAFR). We find that the NAFR mechanism plays the largest role, while the ODT mechanism is absent in our simulations as La Niña-like rather than El-Niño-like conditions develop following a uniform radiative forcing over the equatorial Pacific.

Disentangling the mechanisms of ENSO response to tropical volcanic eruptions

Francesco S.R. Pausata[1*], Yang Zhao[2], Davide Zanchettin[3],
Rodrigo Caballero[4] and David S. Battisti[5,6]

Affiliations

[1]Centre ESCER (Étude et la Simulation du Climat à l'Échelle Régionale) and GEOTOP (Research Center on the dynamics of the Earth System), Department of Earth and Atmospheric Sciences, University of Quebec in Montreal, Montreal, QC H3C 3J7, Canada

[2] State Key Laboratory of Severe Weather, Chinese Academy of Meteorological Sciences, Beijing, China

[3]Department of Environmental Sciences, Informatics and Statistics, University Ca'Foscari of Venice, Mestre, Italy

[4]Department of Meteorology, Stockholm University and Bolin Centre for Climate Research, Stockholm, Sweden,

[5]Department of Atmospheric Sciences, University of Washington, Seattle, Washington, USA

[6]UNI Research, Bergen, Norway

*Corresponding author: Francesco S.R. Pausata (pausata.francesco@uqam.ca)

Key points

- The cooling of tropical northern Africa is a key mechanism to explain the occurrence of a post-eruption El Niños.
- The "ocean thermostat mechanism" is absent in our simulations and cannot explain the post-eruption El Niño tendency as previously suggested.
- The Maritime Continent cooling mechanism is not at play when the aerosol forcing extends over the entire equatorial Pacific.

Abstract

Stratospheric volcanic aerosol can have major impacts on global climate. Despite a consensus among studies on an El Niño–like response in the first or second post-eruption year, the mechanisms that trigger a change in the state of El Niño-Southern Oscillation (ENSO) following volcanic eruptions are still debated.

Here, we shed light on the processes that govern the ENSO response to tropical volcanic eruptions through a series of sensitivity experiments with an Earth System Model where a uniform stratospheric volcanic aerosol loading is imposed over different parts of the tropics. Three tropical mechanisms are tested: the "ocean dynamical thermostat" (ODT); the cooling of the Maritime Continent; and the cooling of tropical northern Africa (NAFR). We find that the NAFR mechanism plays the largest role, while the ODT mechanism is absent in our simulations as La Niña-like rather than El-Niño-like conditions develop following a uniform radiative forcing over the equatorial Pacific.

1. Introduction

Large explosive volcanic eruptions can have major impacts on global climate, affecting both radiative balance and inducing interannual-to-decadal dynamical alterations of the atmospheric and ocean circulation [e.g., *Timmreck*, 2012; *Zanchettin*, 2017]. Such impacts are mainly due to the injection of large quantities of sulfur dioxide into the stratosphere, which are oxidized and then converted into sulfate aerosols. Consequently, the stratospheric aerosol layer is enhanced for 2-3 years following major eruptions, during which the aerosol scatters some incoming solar radiation back to space cooling the surface [e.g., *Timmreck*, 2012].

The global average surface cooling reaches its maximum 6–18 months after the peak net direct radiative forcing corresponding to the maximum enhancement of the stratospheric volcanic aerosol layer [*Thompson et al.*, 2009]. Volcanic eruptions induce dynamical responses in the Earth system as well, which are seen as modulation of natural modes of climate variability, such as the Arctic Oscillation/North Atlantic Oscillation [*Kodera*, 1994; *Shindell et al.*, 2004; *Christiansen*, 2008] and the El Niño–Southern Oscillation (ENSO) [*Emile-Geay et al.*, 2008; *McGregor and Timmermann*, 2011]. Given the profound influence of ENSO on global climate and its strong societal relevance, it is important to understand how volcanism can modulate ENSO. Such understanding may enhance predictability of subsequent El Niño/La Niña events following future volcanic eruptions.

Despite some discrepancies across studies regarding the response of ENSO to volcanic forcing based on paleoclimate reconstructions [e.g., *Adams et al.*, 2003; *Li et al.*, 2013; *Dee et al.*, 2020], *McGregor et al.* [2020] showed that the majority of available reconstructions (12 out of 17 reconstructions) display an El Niño–like warming in the year of eruption, while none display a significant La Niña–like response when provided with consistent dates of volcanic eruptions. Furthermore, *McGregor et al.* [2020] identify an emerging consensus from the numerous coupled General Circulation Model (CGCM) studies investigating the impact of tropical volcanism on ENSO, with the overwhelming majority displaying an El Niño–like warming in the year following the eruption. However, different aerosol spatial distributions, hence differences in the spatial structure of volcanic forcing, may trigger different ENSO responses. Stevenson *et al.* [*Stevenson et al.*, 2016] investigated the impact of Northern Hemisphere (NH), Southern Hemisphere (SH) and tropical volcanic eruptions using the Community Earth System Model - Last Millennium Ensemble (CESM-LME). They concluded that while NH and tropical eruptions tend to favour El Niño-like conditions, SH eruptions enhance the probability of La Niña-like events within one year from the eruptions. Similar results were found by *Pausata et al.*, [2020] and *Ward et al.* [2021] using different CGCMs (NorESM1-M and MPI-ESM, respectively). Conversely, *Zuo et al.* [2018], also using the CESM-LME, concluded that SH, NH and tropical eruptions all resulted in El Niño-like conditions in the year of the eruption – albeit weak for SH eruptions. However, Zuo *et al.* [*Zuo et al.*, 2018] define ENSO anomalies relative to zonal mean cooling, introducing methodological specificities, particularly regarding the separation of dynamical ENSO responses from tropical radiative cooling, that may in part explain differences with previously published results.

The mechanisms that trigger changes in the ENSO state following volcanic eruptions are still debated. When an eruption results in an aerosol distribution with strong hemispheric asymmetry, the impact on the evolution of ENSO is robust across models and is mostly governed by energetic constraints [*Kang et al.*, 2008; *Schneider et al.*, 2014]. The associated asymmetric cooling of the hemispheres features meridional shifts in the Intertropical Convergence Zone (ITCZ) [*Atwood et al.*, 2020] and subsequent coupled atmosphere-ocean feedbacks in the tropical Pacific [*Pausata et al.*, 2015b, 2016, 2020; *Colose et al.*, 2016; *Stevenson et al.*, 2016]. An eruption, yielding aerosol that is concentrated in the NH, moves the ITCZ in the Pacific equatorward, weakening the trade winds and leading to an El Niño-like anomaly via the Bjerknes feedback. In contrast, aerosol concentrated in the SH moves the ITCZ northward inducing a strengthening of the trade winds along the equator, hence triggering La Niña-like anomalies.
The mechanisms triggering the ENSO response to a tropical eruption that results in a weak hemispheric asymmetry are not hitherto fully understood, however. One of the most frequently adopted hypotheses is the "ocean dynamical thermostat" mechanism (ODT) [*Clement et al.*, 1996], where a uniform negative radiative forcing over the equatorial Pacific initially induces less cooling in the eastern relative to the western Pacific due to the presence of strong ocean upwelling in the eastern Pacific, which helps maintain the sea-surface temperature (SST) there close to the temperature of the upwelling water. The weakened zonal SST gradient along the equatorial Pacific causes a relaxation of the trade winds and reduces the ocean upwelling in the eastern Pacific. This process is then amplified by the Bjerknes feedback, resulting in an El Niño response to volcanic forcing [*Bjerknes*, 1969]. The ODT mechanism emerged in simulations with an idealized model [the Zebiak-Cane model [*Zebiak and Cane*, 1987]] and an imposed uniform radiative cooling [*Hirono*, 1988; *Clement et al.*, 1996; *Mann et al.*, 2005; *Emile-Geay et al.*, 2008]. However, recent studies have questioned the existence of the ODT mechanism in CGCMs [e.g., *Stevenson et al.*, 2016; *Pausata et al.*, 2020; *Ward et al.*, 2021].

Another suggested mechanism for the ENSO response to a tropical aerosol forcing is based on the land-ocean temperature gradient [*Ohba et al.*, 2013; *Predybaylo et al.*, 2017], which is enhanced after a volcanic eruption as land areas (e.g., the Maritime Continent [*Ohba et al.*, 2013] or Southeast Asia [*Predybaylo et al.*, 2017]) initially cools faster than the ocean. The increased land-ocean temperature gradient would then initiate a westerly wind anomaly in the western equatorial Pacific, leading to an El Niño–like anomaly through the Bjerknes feedback.
Finally, *Khodri et al.* [2017] proposed a mechanism whereby atmospheric teleconnections are the source of an altered Walker circulation in post-eruption years. According to this mechanism, the reduction of the tropical precipitation over Africa and tropospheric cooling causes anomalous atmospheric Kelvin waves in boreal fall that weaken the trade winds over the western Pacific, leading to El Niño-like conditions in the year after a major eruption. However, there is no consensus yet as to which of these proposed mechanisms is the main driver of the ENSO response after large tropical volcanic eruptions.

Here, we design and perform a series of sensitivity experiments to isolate each of the three tropical mechanisms that have been brought forward for the ENSO response to tropical volcanic eruptions. Specifically, in our experiments we perform "volcano" experiments in which we impose a uniform spatially fixed aerosol loading over different parts of the tropics (Fig. 1) starting in June and lasting for about 1.5 years (Fig. S1). These experiments are meant to shed light on the processes that govern the ENSO response as a function of the regional distribution of the aerosol forcing.

2. Model Description and Experimental Setup

2.1 Model description

We used the Norwegian Earth System Model (NorESM1-M [*Bentsen et al.*, 2013; *Iversen et al.*, 2013]) to simulate a set of sensitivity experiment in which we prescribe aerosol concentrations over specific areas of the tropics to test the above-mention mechanisms that could potentially trigger the post-volcano ENSO response. NorESM1-M has a horizontal resolution of 1.9° (latitude) × 2.5° (longitude) and 26 vertical levels and uses a modified version of Community Atmospheric Model version 4 (CAM4 [*Neale et al.*, 2013]), CAM4-Oslo, to simulate the atmospheric circulation with an updated module that simulates the life cycle of aerosol particles, and primary and secondary organics. NorESM1-M includes treatment of the direct effect of aerosols and the first and second indirect effects of aerosols on warm clouds [*Kirkevåg et al.*, 2013]. The atmospheric model is coupled to the Miami Isopycnic Coordinate Ocean Model (MICOM), which has a horizontal resolution of ~1.125° along the equator and 53 vertical levels. A detailed description of the model used in this study can be found in *Bentsen et al.* [2013] and *Iversen et al.* [2013]. NorESM is among the best performing coupled climate models in representing ENSO relative to the mean climate state of the tropical Pacific and the spectrum of ENSO variability [*Bellenger et al.*, 2014]. Relative to other climate models, NorESM does not suffer an acute double-ITCZ bias in its climatological mean state [*Bentsen et al.*, 2013; *Pausata et al.*, 2015a] that is widely believed to compromise the model's ability to simulate realistic ENSO variability.

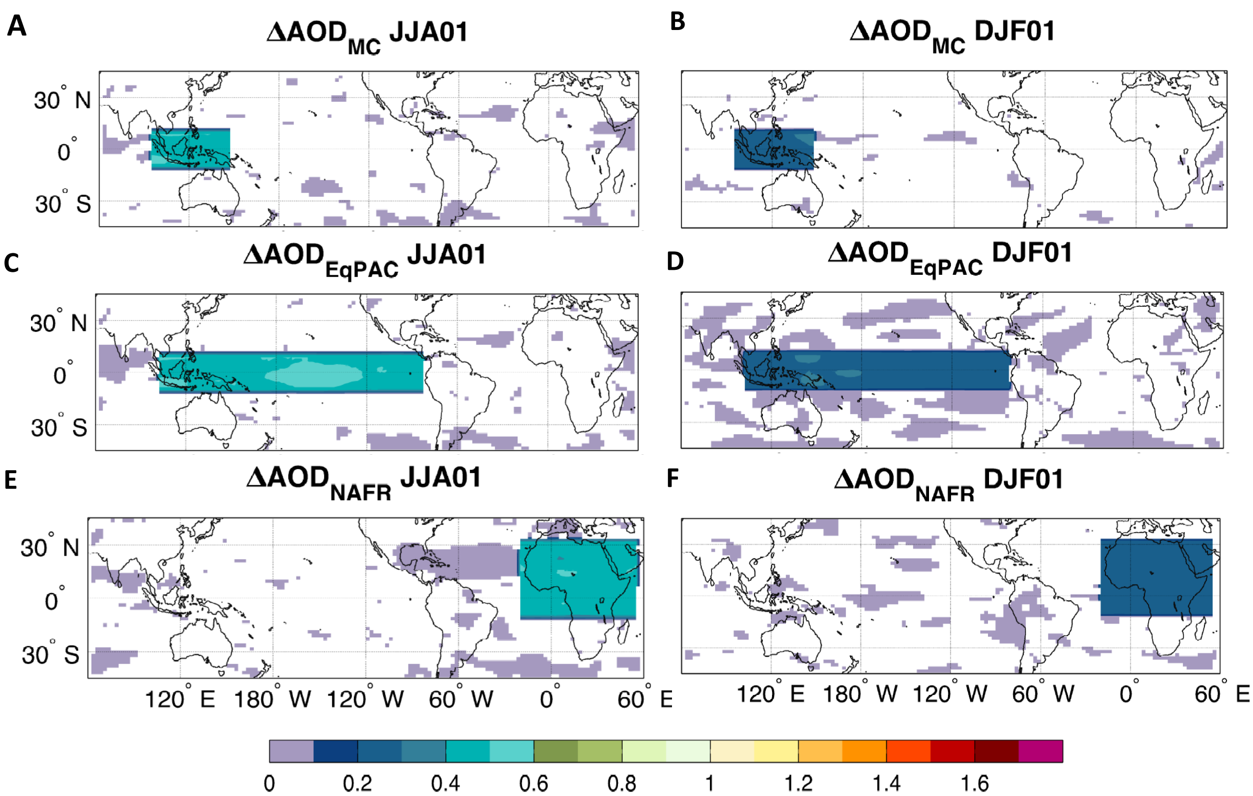

Figure 1. Volcanic forcing. Anomalies in aerosol optical depth (AOD) relative to the no volcano experiment NV. Forcing is localized to the (top) Maritime Continent MC, (middle) the Equatorial Pacific EqPAC, and (middle) tropical and northern Africa – NAFR (bottom). The forcing is applied on 1 June, and anomalies are shown for the summer (June to August, JJA; left) and winter (December to February, DJF; right) following the imposed changes in AOD.

2.2 Experimental design

We performed a series of experiments of 40 ensemble simulations each starting from two specific instants in time selected from a historical transient run forced by anthropogenic greenhouse gas and aerosol forcing from 1850 – 2005. These two initial conditions from the transient simulation are used in both our aerosol forcing experiments ("volcano case") and in the reference volcanically-unperturbed experiments ("no-volcano", NV) where the volcanic aerosol concentration is set to background conditions: 1 June 1923 and 1 June 1927. We chose 1 June 1923 as our starting date because the tropical Pacific is in an ENSO neutral state (Niño3.4 index = −0.1°C in June), but in the absence of an eruption is trending to La Niña conditions 3 months later (Niño3.4 index = −0.4°C in September; see Fig. 2A in *Pausata et al.* [2020]). Unlike for 1 June 1923, the 1 June 1927 volcanic eruption is imposed upon a warm ENSO state (Niño3.4 index = +0.4°C) that, if not perturbed, remains warm for the next 18 months (see Fig. 2A in *Pausata et al.* [2020]). The two different initial ENSO states allow to account for uncertainty in the ENSO response due to ocean preconditioning [*Pausata et al.*, 2016; *Predybaylo et al.*, 2020]. For each of the two initial conditions, 20 simulations are performed with slightly modified initial conditions. The difference between the ensemble mean climate state induced by prescribing volcano aerosol forcing (MC, EqPAC or NAFR) and the unperturbed climate state (NV) shows the time history of the response to that forcing in terms of paired anomalies [*Pausata et al.*, 2015a; *Zanchettin et al.*, 2022] and illuminates the impact of forcing on the evolution of ENSO. For example, the change in surface temperature (TS) due to forcing over the Maritime Continent, net of the natural evolution of the unperturbed climate system, is $\Delta TS_{MC} = T_{MC} - T_{NV}$. Figures in the paper show the average response over all 40 ensemble members.

The volcano experiments are highly idealized experiments in which a prescribed aerosol forcing is imposed in different areas of the tropics through prescribed changes in the aerosol mass mixing ratio. The imposed aerosol mass mixing ratio corresponds to an aerosol optical depth (AOD) anomaly peaking in August/September at about 0.4/0.5 at 550 nm either over the equatorial Pacific (EqPAC), the Maritime Continent (MC) or tropical and northern Africa (NAFR). The resulting radiative forcing peaks in the first post-eruption summer and it amounts to about -8 W/m^2 in the region where the volcanic aerosol forcing is applied (Fig. S1); and the forcing fades away returning to background AOD values after 1.5 years. The imposed AOD anomaly corresponds to the zonal mean AOD anomaly estimated in the tropical regions following a Tambora eruption [*Zanchettin et al.*, 2016a]. As we imposed the aerosol mass mixing ratio anomalies over specific areas, there is no transport of volcanic aerosols outside the forcing region. We perform two additional experiments in which extreme AOD anomalies (~3 times larger than in the previous case) are applied over the Maritime Continent (MCext) and the Equatorial Pacific (EqPACext) to account for the fact that many tropical eruptions occur in the Maritime Continent, where much higher aerosol concentrations than the zonal average typically develop, particularly in the first post-eruption months (Fig. S2). The maximum radiative forcing of about -22 W/m^2 peaks in September of the first post-eruption year (Fig. S1). The prescribed SO_4 gradient at the borders of the forcing regions where the aerosol forcing is imposed is not dissimilar from the gradients that develop in experiments where the volcanic plume is allowed to evolve [see for example Fig. 2, A and B, in the TrNH eruptions in *Pausata et al.* [2020]. Therefore, it does not, in itself, present an additional or unique unrealistic forcing that could unduly affect the results.

In the MC experiments, we prescribe an increased SO_4 mixing ratio over the region between 10°S to 10°N and 100°E to 150°E, and we extend it to cover 100°E to 80°W in the EqPAC experiment. In the NAFR experiments the imposed aerosol forcing extends from 10°S to 33°N and from 20°W to 55°E. We opted for prescribing the aerosol forcing over the specific area of interest rather than simulating interactively a volcanic eruption to test the above-mentioned mechanisms. This experimental design precludes extratropical forcing and hemispheric asymmetry in forcing that would accompany any tropical eruption by way of the Brewer-Dobson circulation [*Toohey et al.*, 2011] and, thus, isolates the impact of tropical aerosol forcing.

Hereafter, for simplicity we refer to "eruption" when discussing the various experiments in which we apply a uniform (regional) aerosol forcing.

The ENSO index used in this study is based on monthly SST anomalies averaged over the Niño3.4 region (5°N to 5°S; 170°W to 120°W). We apply a 5-month running mean to remove intraseasonal variations in SST. An El Niño event is defined when the Niño3.4 index exceeds 1 SD (+0.4°C) for at least 6 consecutive months. Unless otherwise noted, all differences discussed in this study are significant at the 95% confidence level using a Student's *t* test.

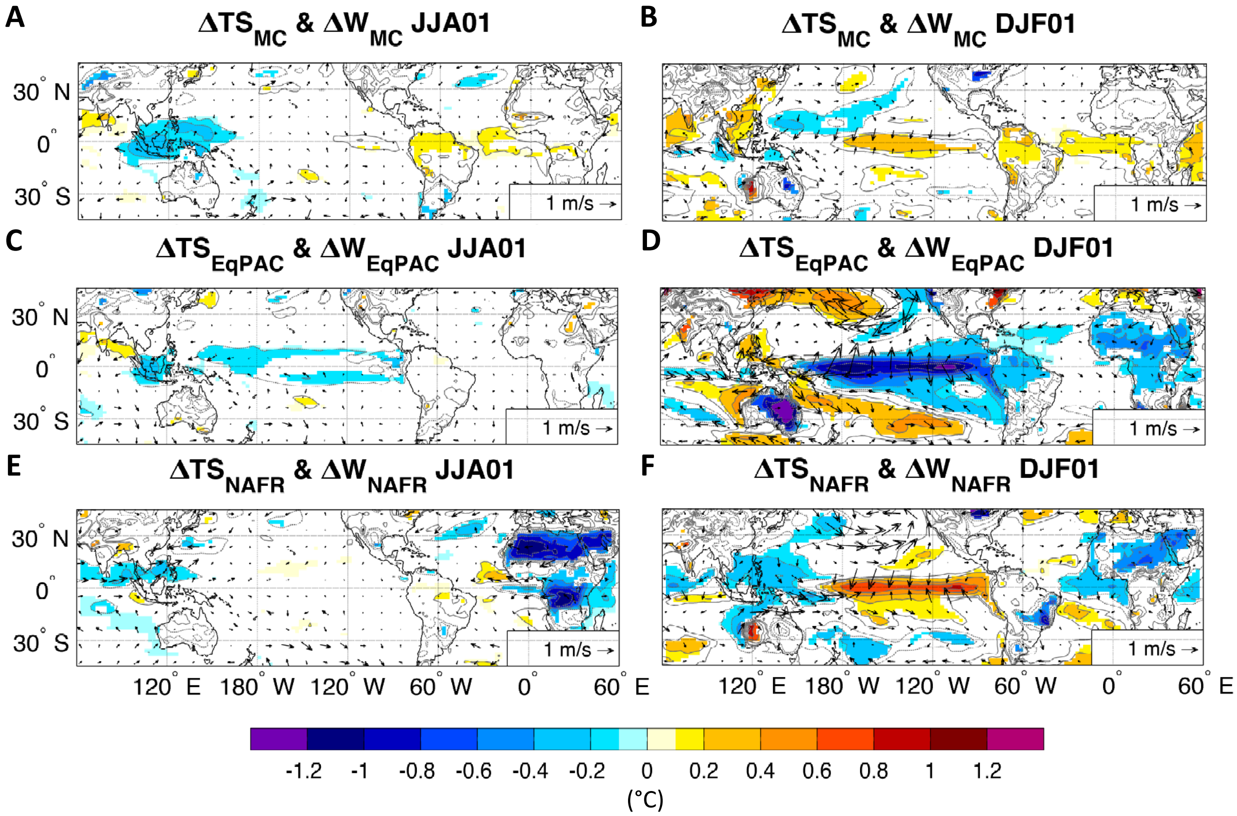

Figure 2. Surface temperature and wind response. Changes in surface temperature (°C, contours and shadings) and wind (m/s, arrows) in the summer (June to August – JJA; left) and winter (December to February – DJF; right) following the AOD imposed anomalies above the Maritime Continent - MC (A and B), the equatorial Pacific - EqPAC (C and D), and the tropical and northern Africa – NAFR (E and F) relative to the no-volcano experiment. Only temperature values that are significantly different at the 5% level using a local (grid-point) *t* test are shaded. The contours follow the colorbar intervals (solid for positive and dashed for negative anomalies; the zero line is omitted).

3. Results

3.1 The MC cooling and ODT mechanisms

When a uniform stratospheric volcanic aerosol loading is applied over the Maritime Continent (MC experiment) a cooling is simulated over the entire region following the eruption (Fig. 2A). The MC cooling triggers weak westerly wind anomalies (Figs. 2A and S3A) as an area of low-level divergence develops over the Maritime Continent (Fig. S3A). These changes then give rise to a modest El Niño-like response in the first post-eruption winter (Fig. 2B). The warm anomalies fade away by the end of the spring and La Niña-like conditions start developing in the second post-eruption summer (Figs. 3 and S4B).

When the aerosol loading is extended to the entire equatorial Pacific (EqPAC experiment), the surface response in the equatorial Pacific is a weak cooling during the first three months when the volcanic aerosol anomalies are imposed (Figs. 2C and 3). The cooling extends from the western seaboard of South America to the Maritime Continent (Fig. 2C) and is accompanied by a weak intensification of the trade winds (Figs 2C and S3C). The intensification of the trade winds over the central and western tropical Pacific seems to be related to an anomalous zone of convergence that develops in the western Indian Ocean (Figs. 4C and S3C). These results are opposite to what would occur if the ODT mechanism were the dominant reason for the changes in the evolution of ENSO after a tropical eruption. The easterly wind anomalies intensify in the following months and La Niña-like conditions develop in the first post-eruption winter (Figs. 2D and S5C). The cooling is not restricted to the surface and therefore a simple direct response to the radiative forcing, but it extends deeper till the thermocline, showing the classical La Niña pattern (Fig. S5C). The cold anomalies over the equatorial Pacific persist into the following year peaking in the second fall after the eruption (Figs. 2 and S5D).

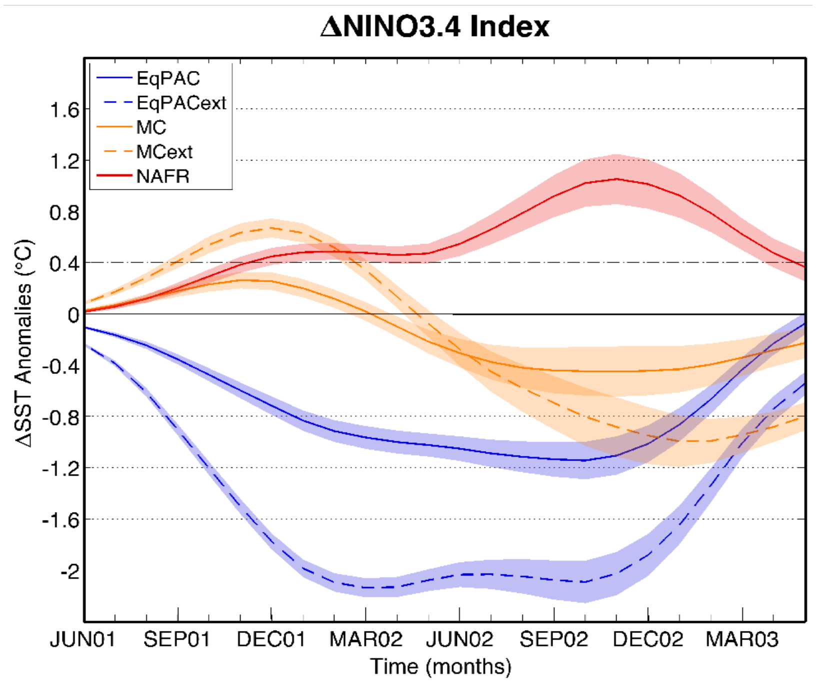

Figure 3. Simulated ENSO response. Changes in the Niño3.4 index for each ensemble experiment relative to the no-volcano case. Shading represents twice the standard error of the mean (approximate 95% confidence intervals).

The temperature and precipitation anomalies following the eruption are not confined to the area where the forcing is applied but spread across the world following – to a large extent – the classical ENSO teleconnections (Figs. 2 and 4). In the MC experiment the global anomalies are weak and resemble those associated with an El Niño event, with wetting over the central western Pacific, and drying over the western Maritime Continent, northern and western Australia, and northern Brazil (Fig. 4, A and B). In the EqPAC experiment, where a La Niña-like response takes place in the boreal winter, the anomalies are mostly of opposite sign compared to the MC experiment. The ITCZ also shifts northward in the Pacific Ocean (Fig. 4, C and D).

Repeating the MC and EqPAC experiments but with extreme aerosol loading (called MCext and EqPACext, respectively) shows similar spatial patterns of SST and precipitation anomalies but with larger amplitude (cf. Figs. 2 and 4 to S6 and S7): a moderate El Niño-like response for the MCext experiment and a very intense La Nina-like response (with cooling exceeding 2°C) developing in the EqPACext ensemble (Figs. 3 and S6).

3.2 The tropical and northern African cooling

In the NAFR experiment the aerosol loading is confined from northern Africa to 10°S (Fig. 1, E and F). The AOD anomalies cause a cooling of up to 1–1.2°C over the Sahara region and south of the equator (Fig. 2E). The cooling causes a drying of about 1 to 2 mm/day in the sub-Saharan regions (Fig. 4E). The reduction in rainfall and the cooling around the equatorial regions in Africa cause a Matsuno–Gill response (Gill, 1980) that alters the Walker Circulation (Fig. S3E) and induces easterly wind anomalies over the Atlantic and westerly wind anomalies over the equatorial Indian and western Pacific Oceans (Figs. 2E and S3E). The shift in the Walker circulation leads to a reduced convection over the western Pacific that further strengthens the westerly wind signal (Figs. 2F and S3F). In the equatorial Atlantic, an Atlantic Niña-like develops due to the easterly wind anomalies shallowing the thermocline. The westerly wind anomaly in the western equatorial Pacific triggers oceanic downwelling Kelvin waves that travel eastward reaching the eastern Pacific in the winter following the eruption (Fig. S5E). The anomalous Kelvin waves deepen the thermocline in the central and eastern Pacific (Fig. S5E) contributing to the development of an El Niño. During the summer of the following year, the cooling and drying over tropical northern Africa is no longer present. However, persistence of the Atlantic La Niña-like anomaly (Fig. S8e) contributes to enhancing westerly wind anomalies over the Pacific (Fig. S5e), favoring the continuation of El Niño-like conditions as pointed out in recent studies [*Rodríguez-Fonseca et al.*, 2009; *Li et al.*, 2016; *Zanchettin et al.*, 2016b; *Pausata et al.*, 2017].

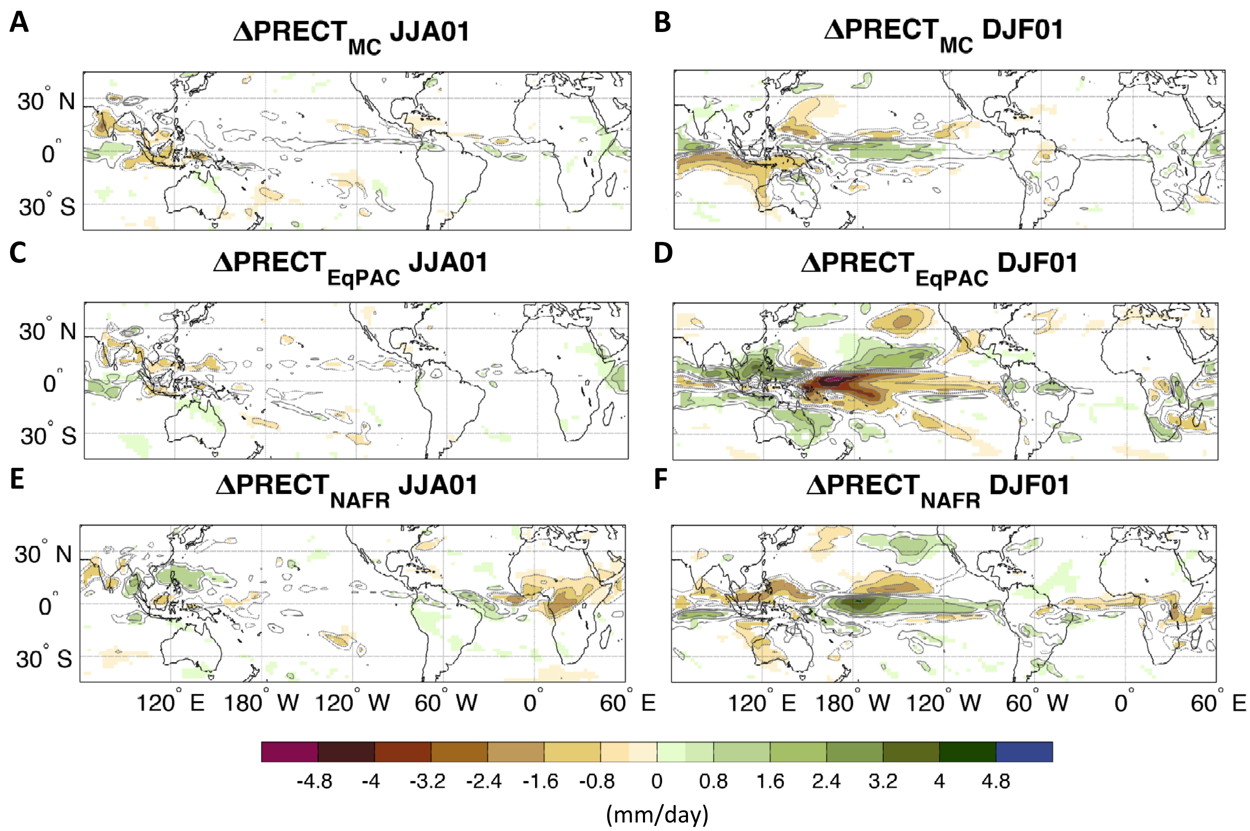

Figure 4. Rainfall response. Changes in precipitation (mm/day, contours and shadings) in the first summer (June to August – JJA; left) and winter (December to February – DJF; right) following the AOD imposed anomalies above the Maritime Continent – MC (A and B), the equatorial Pacific – EqPAC (C and D) and the tropical and northern Africa – NAFR (E and F) relative to the no-volcano experiment. Only precipitation values that are significantly different at the 5% level using a local (grid-point) *t* test are shaded. The contours follow the colorbar intervals (solid for positive and dashed for negative anomalies; the zero line is omitted).

The results from the NAFR experiment are in broad agreement with the study of *Khodri et al.* [2017], who also found that the cooling and drying of tropical Africa initiate westerly wind anomalies over western Pacific oceans able to affect ENSO for two consecutive years, and additionally point to a possible westward pathway for the northern African mechanism through the Atlantic Niña phenomenon.

4. Discussion and Conclusions

This study provides the first attempt to disentangle different mechanisms governing the ENSO response to volcanic forcing through idealized coupled climate model experiments where the volcanic aerosol is confined regionally. The rationale is that regionally confined aerosol loading initiates regionally confined surface cooling. Accordingly, three mechanisms can be tested by our approach, all operating through radiatively forced changes in surface temperature, namely the "ocean dynamical thermostat" (ODT); 2) the cooling of the Maritime Continent (MC); and 3) the cooling of tropical northern Africa (NAFR) mechanism. Among the three mechanisms investigated here, our results point to the tropical northern Africa (NAFR) and the Maritime Continent (MC) as the regions over which the cooling induced by aerosol forcing increases the likelihood of El Niño events following volcanic eruptions. The MC cooling mechanism is in principle able to explain the tendency for positive ENSO phases following volcanic eruptions: El Niño-like anomalies are indeed simulated following a differential cooling between the Maritime Continent and the central-western Pacific Ocean (Fig. 2A). The MC mechanism requires stronger forcing than the NAFR mechanism to be detected (see the MCext experiment) and it relies on the land cooling faster than the ocean. However, when the aerosol forcing is extended to the nearby equatorial Pacific as in the EqPAC (Fig. 1C), the MC does not cool more than the ocean, whereas a uniform cooling spreads from the western to the eastern side of the basin (Figs. 2A and S5) and La Niña-like anomalies subsequently develop. Therefore, the MC cooling mechanism does not work when the volcanic aerosol extends well into the equatorial Pacific, which is usually the case following tropical volcanic eruptions [*Zanchettin et al.*, 2016a]. Furthermore, our EqPAC experiment also highlight that the preferential cooling of the western Pacific ocean relative to the eastern equatorial Pacific, the signature of the ODT mechanism that would give rise to El Niño-like anomalies, does not occur. One possible explanation is that uniform aerosol forcing over the tropical Pacific causes important anomalies in convection over the Indian Ocean that enhance the trade winds in the Pacific, triggering La Niña-like anomalies. However, the Indian Ocean response was not included in the ODT mechanism. Another reason could be related to the fact that in the studies using the Zebiak-Cane model [*Clement et al.*, 1996; *Mann et al.*, 2005; *Emile-Geay et al.*, 2008] the uniform forcing (cooling) is imposed at the ocean surface, whereas in our case we impose a uniform forcing in the stratosphere. Because of the more extensive climatological cloud cover in the equatorial western compared to eastern Pacific, the forcing at the ocean surface associated with a volcanic eruption will be weaker there than in the eastern Pacific, which would act to counteract the ODT mechanism and give rise to a more uniform SST cooling.

Based on current understanding, the development of an El Niño response following volcanic eruptions is likely associated with eruptions in which the aerosol loading is either spread rather uniformly across the hemispheres or is mostly confined to the Northern Hemisphere (NH). Such aerosol distributions allow a cooling of northern Africa as well as a larger cooling of the NH relative to the Southern Hemisphere, which will also trigger a southward displacement of the ITCZ [*Pausata et al.*, 2015b, 2020; *Ward et al.*, 2021]. Both mechanisms – NAFR cooling and southward ITCZ shift - will constructively superpose to trigger a weakening of the trades along the equatorial Pacific and therefore lead to El Niño-like anomalies. Pausata *et al.* [*Pausata et al.*, 2020] also suggest a potential role of the extratropics in which the extratropical response to volcanic aerosol radiative forcing mediates the ENSO response favoring El Niño-like anomalies. Our sensitivity experiments allow to evaluate individually mechanisms of ENSO response to volcanic forcing; however, in the real world the ENSO response is a combination – non necessary linear – of all such mechanisms, whose individual relative role may also be significantly affected by background climate conditions.

Our study provides cues for the design of coordinated multi-model experiments to understand the mechanisms underlying the climate response to volcanic eruptions and their different representation in different numerical models. Currently, the Model Intercomparison Project on the climatic response to Volcanic forcing (VolMIP, [*Zanchettin et al.*, 2016a]) tackles questions related to the spatial structure of the forcing only by considering idealized eruptions where the volcanic aerosol is confined either in the northern or the southern hemisphere. Whereas these experiments can shed light on the role of the ITCZ mechanism [*Pausata et al.*, 2020], idealized forcing experiments with regionally-confined aerosol seem necessary to determine whether the ENSO response to volcanic forcing stems from a robust combination of mechanisms in different climate models. Ultimately, this will increase confidence about the predictability of ENSO during periods of strong volcanism.

References:

Adams, J. B., M. E. Mann, and C. M. Ammann (2003), Proxy evidence for an El Niño-like response to volcanic forcing., *Nature*, *426*(6964), 274–8, doi:10.1038/nature02101.

Atwood, A. R., A. Donohoe, D. S. Battisti, X. Liu, and F. S. R. Pausata (2020), Robust Longitudinally Variable Responses of the ITCZ to a Myriad of Climate Forcings, *Geophys. Res. Lett.*, *47*(17), e2020GL088833, doi:10.1029/2020GL088833.

Bellenger, H., E. Guilyardi, J. Leloup, M. Lengaigne, and J. Vialard (2014), ENSO representation in climate models: from CMIP3 to CMIP5, *Clim. Dyn.*, *42*(7–8), 1999–2018, doi:10.1007/s00382-013-1783-z.

Bentsen, M. et al. (2013), The Norwegian Earth System Model, NorESM1-M – Part 1: Description and basic evaluation of the physical climate, *Geosci. Model Dev.*, *6*(3), 687–720, doi:10.5194/gmd-6-687-2013.

Bjerknes, J. (1969), Atmospheric teleconnections from the equatorial Pacific, *Mon. Weather Rev.*, *97*(3), 163–172, doi:10.1175/1520-0493(1969)097<0163:ATFTEP>2.3.CO;2.

Christiansen, B. (2008), Volcanic Eruptions, Large-Scale Modes in the Northern Hemisphere, and the El Niño–Southern Oscillation, *J. Clim.*, *21*(5), 910–922, doi:10.1175/2007JCLI1657.1.

Clement, A. C., R. Seager, M. A. Cane, and S. E. Zebiak (1996), An Ocean Dynamical Thermostat, *J. Clim.*, *9*(9), 2190–2196, doi:10.1175/1520-0442(1996)009<2190:AODT>2.0.CO;2.

Colose, C. M., A. N. LeGrande, and M. Vuille (2016), Hemispherically asymmetric volcanic forcing of tropical hydroclimate during the last millennium, *Earth Syst. Dyn.*, *7*(3), 681–696, doi:10.5194/esd-7-681-2016.

Dee, S. G., K. M. Cobb, J. Emile-Geay, T. R. Ault, R. L. Edwards, H. Cheng, and C. D. Charles (2020), No consistent ENSO response to volcanic forcing over the last millennium, *Science (80-.).*, *367*(6485), 1477–1481, doi:10.1126/science.aax2000.

Emile-Geay, J., R. Seager, M. A. Cane, E. R. Cook, and G. H. Haug (2008), Volcanoes and ENSO over the Past Millennium, *J. Clim.*, *21*(13), 3134–3148, doi:10.1175/2007JCLI1884.1.

Hirono, M. (1988), On the trigger of El Niño Southern Oscillation by the forcing of early El Chichón volcanic aerosols, *J. Geophys. Res.*, *93*(D5), 5365, doi:10.1029/JD093iD05p05365.

Iversen, T. et al. (2013), The Norwegian Earth System Model, NorESM1-M – Part 2: Climate response and scenario projections, *Geosci. Model Dev.*, *6*(2), 389–415, doi:10.5194/gmd-6-389-2013.

Kang, S. M., I. M. Held, D. M. W. Frierson, and M. Zhao (2008), The Response of the ITCZ to Extratropical Thermal Forcing: Idealized Slab-Ocean Experiments with a GCM, *J. Clim.*, *21*(14), 3521–3532, doi:10.1175/2007JCLI2146.1.

Khodri, M. et al. (2017), Tropical explosive volcanic eruptions can trigger El Niño by cooling tropical Africa, *Nat. Commun.*, *8*(1), 778, doi:10.1038/s41467-017-00755-6.
Kirkevåg, A. et al. (2013), Aerosol-climate interactions in the Norwegian Earth System Model - NorESM1-M, *Geosci. Model Dev.*, *6*, 207–244, doi:10.5194/gmd-6-207-2013.
Kodera, K. (1994), Influence of volcanic eruptions on the troposphere through stratospheric dynamical processes in the northern hemisphere winter, *J. Geophys. Res.*, *99*(D1), 1273, doi:10.1029/93JD02731.
Li, J. et al. (2013), El Niño modulations over the past seven centuries, *Nat. Clim. Chang.*, *3*(9), 822–826, doi:10.1038/nclimate1936.
Li, X., S.-P. Xie, S. T. Gille, and C. Yoo (2016), Atlantic-induced pan-tropical climate change over the past three decades, *Nat. Clim. Chang.*, *6*, 275–279, doi:10.1038/nclimate2840.
Mann, M. E., M. A. Cane, S. E. Zebiak, and A. Clement (2005), Volcanic and Solar Forcing of the Tropical Pacific over the Past 1000 Years, *J. Clim.*, *18*(3), 447–456, doi:10.1175/JCLI-3276.1.
McGregor, S., and A. Timmermann (2011), The Effect of Explosive Tropical Volcanism on ENSO, *J. Clim.*, *24*(8), 2178–2191, doi:10.1175/2010JCLI3990.1.
McGregor, S., M. Khodri, N. Maher, M. Ohba, F. S. R. Pausata, and S. Stevenson (2020), The Effect of Strong Volcanic Eruptions on ENSO, in *El Niño Southern Oscillation in a Changing Climate*, pp. 267–287, Geophysical Monograph Series, American Geophysical Union, doi:10.1002/9781119548164.ch12
Neale, R. B., J. Richter, S. Park, P. H. Lauritzen, S. J. Vavrus, P. J. Rasch, and M. Zhang (2013), The Mean Climate of the Community Atmosphere Model (CAM4) in Forced SST and Fully Coupled Experiments, *J. Clim.*, *26*(14), 5150–5168, doi:10.1175/JCLI-D-12-00236.1.
Ohba, M., H. Shiogama, T. Yokohata, and M. Watanabe (2013), Impact of Strong Tropical Volcanic Eruptions on ENSO Simulated in a Coupled GCM, *J. Clim.*, *26*, 5169–5182.
Pausata, F. S. R., A. Grini, R. Caballero, A. Hannachi, and Ø. Seland (2015a), High-latitude volcanic eruptions in the Norwegian Earth System Model: The effect of different initial conditions and of the ensemble size, *Tellus, Ser. B Chem. Phys. Meteorol.*, *67*(26728), doi:10.3402/tellusb.v67.26728.
Pausata, F. S. R., L. Chafik, R. Caballero, and D. S. Battisti (2015b), Impacts of high-latitude volcanic eruptions on ENSO and AMOC, *Proc. Natl. Acad. Sci.*, *112*(45), 13784–13788, doi:10.1073/pnas.1509153112.
Pausata, F. S. R., C. Karamperidou, R. Caballero, and D. S. Battisti (2016), ENSO response to high-latitude volcanic eruptions in the Northern Hemisphere: The role of the initial conditions, *Geophys. Res. Lett.*, *43*(16), 8694–8702, doi:10.1002/2016GL069575.
Pausata, F. S. R., Q. Zhang, F. Muschitiello, Z. Lu, L. Chafik, E. M. Niedermeyer, J. C. Stager, K. M. Cobb, and Z. Liu (2017), Greening of the Sahara suppressed ENSO activity during the mid-Holocene, *Nat. Commun.*, *8*, doi:10.1038/ncomms16020.
Pausata, F. S. R., D. Zanchettin, C. Karamperidou, R. Caballero, and D. S. Battisti (2020), ITCZ shift and extratropical teleconnections drive ENSO response to volcanic eruptions, *Sci. Adv.*, *6*(23), doi:10.1126/sciadv.aaz5006.
Predybaylo, E., G. L. Stenchikov, A. T. Wittenberg, and F. Zeng (2017), Impacts of a Pinatubo-size volcanic eruption on ENSO, *J. Geophys. Res. Atmos.*, *122*(2), 925–947, doi:10.1002/2016JD025796.
Predybaylo, E., G. Stenchikov, A. T. Wittenberg, and S. Osipov (2020), El Niño/Southern Oscillation response to low-latitude volcanic eruptions depends on ocean pre-conditions and eruption timing, *Commun. Earth Environ.*, *1*(1), 12, doi:10.1038/s43247-020-0013-y.
Rodríguez-Fonseca, B., I. Polo, J. García-Serrano, T. Losada, E. Mohino, C. R. Mechoso, and F. Kucharski (2009), Are Atlantic Niños enhancing Pacific ENSO events in recent decades?, *Geophys. Res. Lett.*, *36*(20), L20705, doi:10.1029/2009GL040048.

Schneider, T., T. Bischoff, and G. H. Haug (2014), Migrations and dynamics of the intertropical convergence zone., *Nature*, *513*(7516), 45–53, doi:10.1038/nature13636.

Shindell, D. T., G. A. Schmidt, M. E. Mann, and G. Faluvegi (2004), Dynamic winter climate response to large tropical volcanic eruptions since 1600, *J. Geophys. Res.*, *109*(D5), D05104, doi:10.1029/2003JD004151.

Stevenson, S., B. Otto-Bliesner, J. Fasullo, and E. Brady (2016), "El Niño Like" Hydroclimate Responses to Last Millennium Volcanic Eruptions, *J. Clim.*, *29*(8), 2907–2921, doi:10.1175/JCLI-D-15-0239.1.

Thompson, D. W. J., J. M. Wallace, P. D. Jones, and J. J. Kennedy (2009), Identifying Signatures of Natural Climate Variability in Time Series of Global-Mean Surface Temperature: Methodology and Insights, *J. Clim.*, *22*(22), 6120–6141, doi:10.1175/2009JCLI3089.1.

Timmreck, C. (2012), Modeling the climatic effects of large explosive volcanic eruptions, *Wiley Interdiscip. Rev. Clim. Chang.*, *3*(6), 545–564, doi:10.1002/wcc.192.

Toohey, M., K. Krüger, U. Niemeier, and C. Timmreck (2011), The influence of eruption season on the global aerosol evolution and radiative impact of tropical volcanic eruptions, *Atmos. Chem. Phys.*, *11*(23), 12351–12367, doi:10.5194/acp-11-12351-2011.

Ward, B., F. S. R. Pausata, and N. Maher (2021), The sensitivity of the El Ninõ-Southern Oscillation to volcanic aerosol spatial distribution in the MPI Grand Ensemble, *Earth Syst. Dyn.*, *12*(3), doi:10.5194/esd-12-975-2021.

Zanchettin, D. (2017), Aerosol and Solar Irradiance Effects on Decadal Climate Variability and Predictability, *Curr. Clim. Chang. Reports*, *3*(2), 150–162, doi:10.1007/s40641-017-0065-y.

Zanchettin, D. et al. (2016a), The Model Intercomparison Project on the climatic response to Volcanic forcing (VolMIP): Experimental design and forcing input data for CMIP6, *Geosci. Model Dev.*, *9*(8), doi:10.5194/gmd-9-2701-2016.

Zanchettin, D., O. Bothe, H. F. Graf, N. Omrani, A. Rubino, and J. H. Jungclaus (2016b), A decadally delayed response of the tropical Pacific to Atlantic multidecadal variability, *Geophys. Res. Lett.*, *43*(2), 784–792, doi:10.1002/2015GL067284.

Zanchettin, D., Timmreck, C., Khodri, M., Schmidt, A., Toohey, M., Abe, M., Bekki, S., Cole, J., Fang, S.-W., Feng, W., Hegerl, G., Johnson, B., Lebas, N., LeGrande, A. N., Mann, G. W., Marshall, L., Rieger, L., Robock, A., Rubinetti, S., Tsigaridis, K., and Weierbach, H. (2022): Effects of forcing differences and initial conditions on inter-model agreement in the VolMIP volc-pinatubo-full experiment, *Geosci. Model Dev.*, 15, 2265–2292, doi:10.5194/gmd-15-2265-2022.

Zebiak, S. E., and M. A. Cane (1987), A Model El Nino–Southern Oscillation, *Mon. Weather Rev.*, *115*(10), 2262–2278, doi:10.1175/1520-0493(1987)115<2262:AMENO>2.0.CO;2.

Zuo, M., W. Man, T. Zhou, Z. Guo, M. Zuo, W. Man, T. Zhou, and Z. Guo (2018), Different Impacts of Northern, Tropical, and Southern Volcanic Eruptions on the Tropical Pacific SST in the Last Millennium, *J. Clim.*, *31*(17), 6729–6744, doi:10.1175/JCLI-D-17-0571.1.

Acknowledgments: We would like to acknowledge that the simulations were performed on resources provided by the Swedish National Infrastructure for Computing (SNIC) at NSC. **Funding:** F.S.R.P. acknowledges the financial support from the Natural Sciences and Engineering Research Council of Canada (grant RGPIN-2018-04981) and the Fonds de recherche du Québec–Nature et technologies (2020-NC-268559). **Author Contributions:** F.S.R.P. conceived the study, designed and performed the experiments, analyzed the model output, and wrote the manuscript; Z.Y. and D.Z. analyzed the model output. All authors contributed to the discussion of the results and the writing of the manuscript. **Competing Interests:** The authors declare that they have no competing interests. **Data Availability Statement:** The datasets generated and analyzed in this study is archived in https://figshare.com/s/2468a3c81dbcb30032ce (DOI: 10.6084/m9.figshare.20349090).

AGU PUBLICATIONS

Geophysical Research Letters

Supporting Information for

Disentangling the mechanisms of ENSO response to tropical volcanic eruptions

Francesco S.R. Pausata[1*], Yang Zhao[2], Davide Zanchettin[3], Rodrigo Caballero[4] and David S. Battisti[5,6]

[1]Centre ESCER (Étude et la Simulation du Climat à l'Échelle Régionale) and GEOTOP (Research Center on the dynamics of the Earth System), Department of Earth and Atmospheric Sciences, University of Quebec in Montreal, Montreal, QC H3C 3J7, Canada

[2] State Key Laboratory of Severe Weather, Chinese Academy of Meteorological Sciences, Beijing, China

[3]Department of Environmental Sciences, Informatics and Statistics, University Ca'Foscari of Venice, Mestre, Italy

[4]Department of Meteorology, Stockholm University and Bolin Centre for Climate Research, Stockholm, Sweden,

[5]Department of Atmospheric Sciences, University of Washington, Seattle, Washington, USA

[6]UNI Research, Bergen, Norway

*Corresponding author: Francesco S.R. Pausata (pausata.francesco@uqam.ca)

Contents of this file

Figures S1 to S8

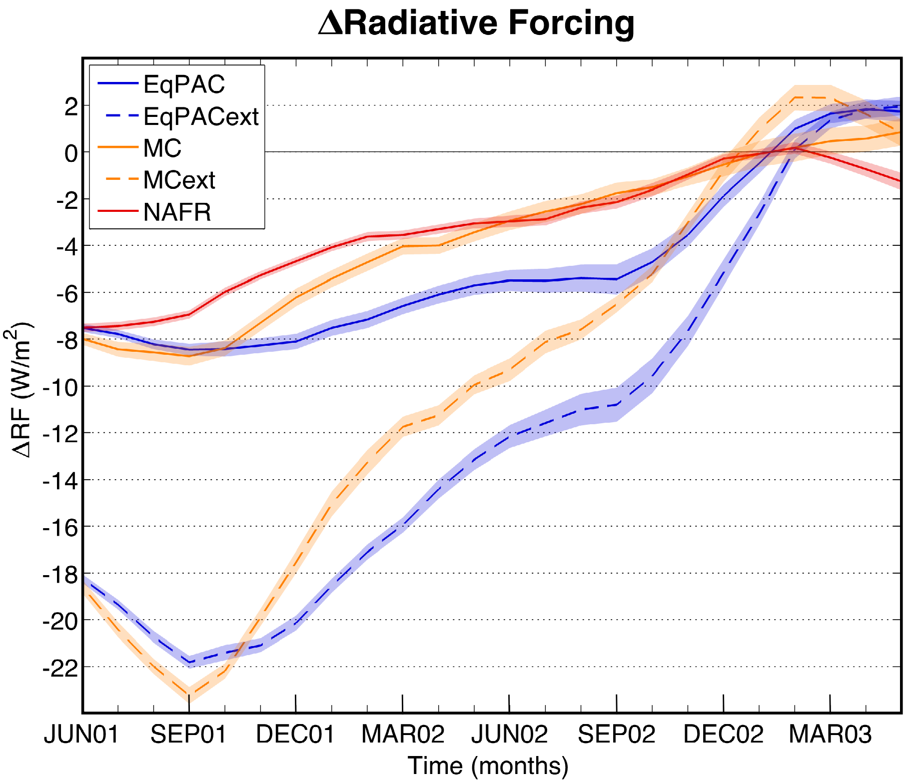

Figure S1. Radiative forcing. Changes in the net radiative forcing at the top of the atmosphere for each ensemble experiment relative to the no-volcano case. Shading represents twice the standard error of the mean (approximate 95% confidence intervals).

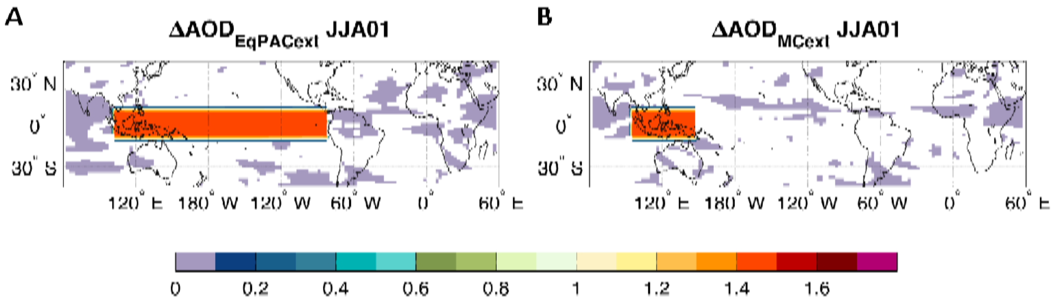

Figure S2. Volcanic forcing in extreme experiments. Anomalies in aerosol optical depth (at 550 nm) in the extreme Maritime Continent – MC experiment (A) and the extreme Equatorial Pacific – EqPAC experiment (B) for the summer (June to August – JJA) following the imposed changes in AOD relative to the no-volcano simulations.

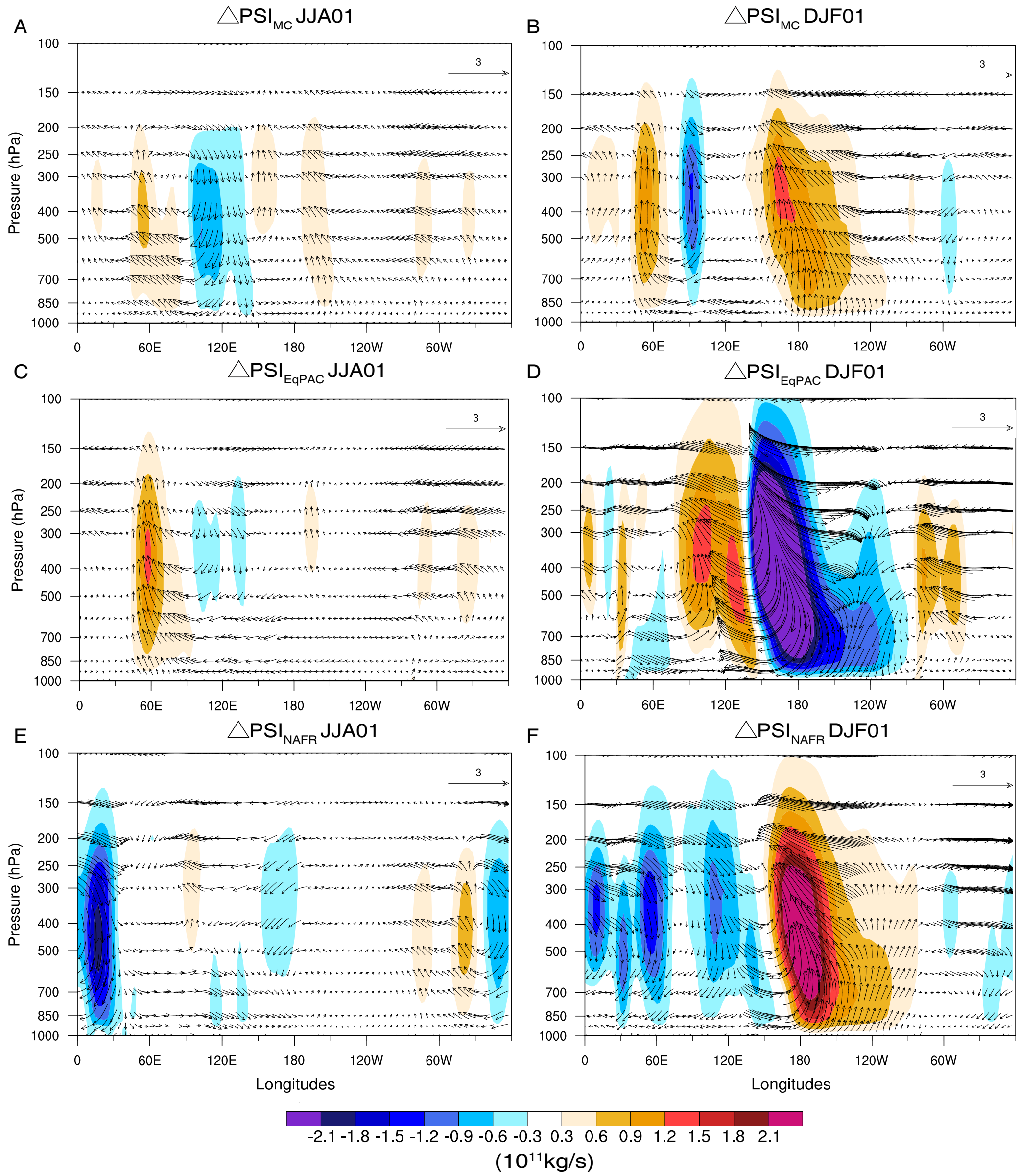

Figure S3. Walker Circulation response in the first post-eruption year. Changes in the zonal stream function (10^{11} kg/s) and vertical winds (m/s) averaged over the Equatorial Pacific (5°S – 5°N) for the first summer (June to August – JJA; left) and winter (December to February – DJF; right) following the AOD imposed anomalies above the Maritime Continent – MC (A - B), the equatorial Pacific – EqPAC (C – D) and the tropical and northern Africa – NAFR (E – F) relative to the no-volcano simulations.

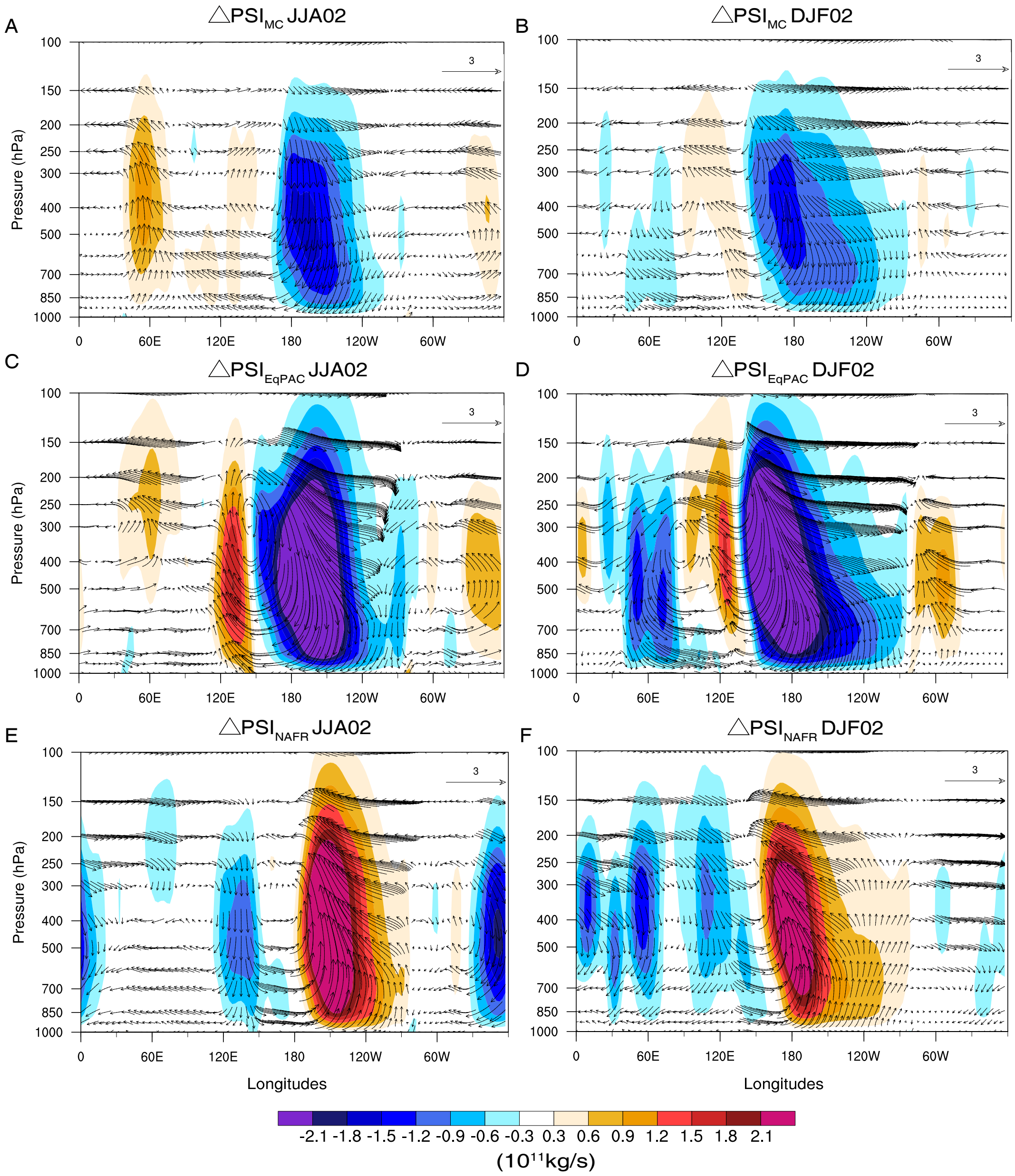

Figure S4. Walker Circulation response in the second post-eruption year. Changes in the zonal stream function (10^{11} kg/s) and vertical winds (m/s) averaged over the Equatorial Pacific (5°S – 5°N) for the second summer (June to August – JJA; left) and winter (December to February – DJF; right) following the AOD imposed anomalies above the Maritime Continent – MC (A and B), the equatorial Pacific – EqPAC (C and D) and the tropical and northern Africa – NAFR (E and F) relative to the no-volcano simulations.

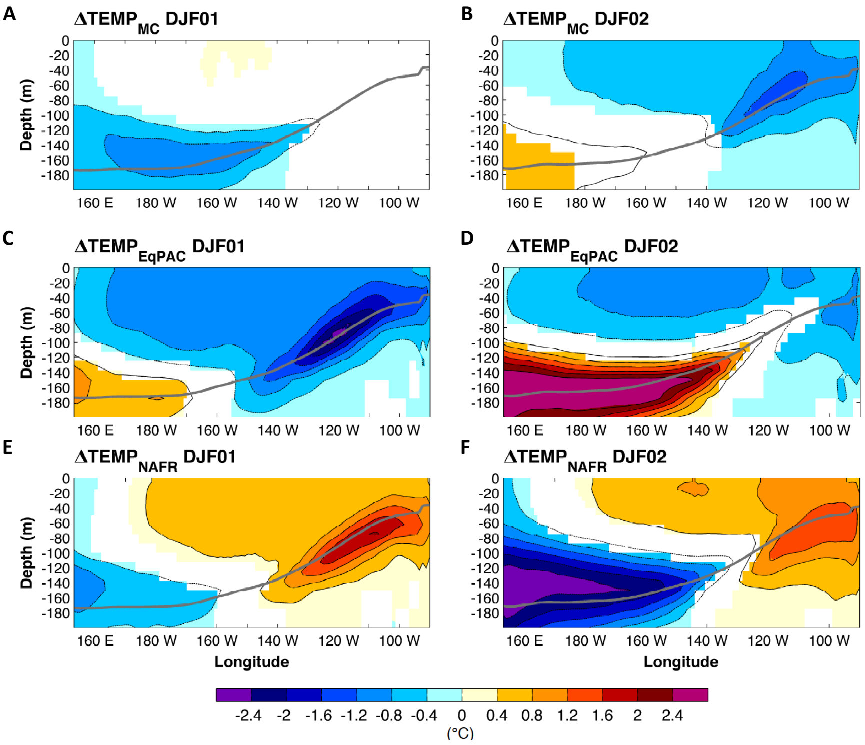

Figure S5. Thermocline response in the first and second post-eruption winter. Ocean temperature (°C) anomalies in the Equatorial Pacific (5°S – 5°N) for the first (left) and second (right) winter (December to February – DJF) following the AOD imposed anomalies over the Maritime Continent – MC (A and B), the equatorial Pacific – EqPAC (C and D) and the tropical and northern Africa – NAFR (E and F) relative to the no-volcano simulations. Only values that are significantly different at the 5% level using a *t* test are shaded. The contours follow the color bar intervals (solid for positive and dashed for negative anomalies; the zero line is omitted). The bold grey line shows the climatological thermocline depth for the no-volcano members (as defined using the 20°C isotherm).

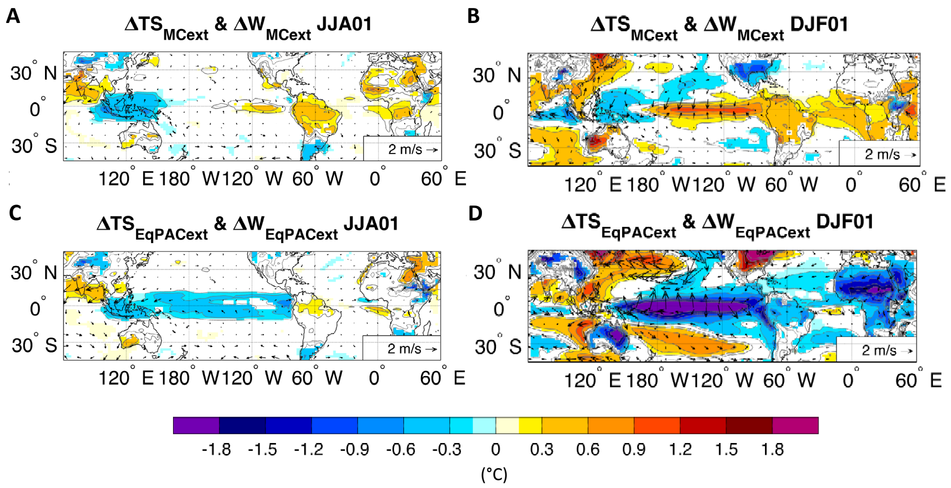

Figure S6. Surface air temperature and wind response for the extreme experiments. Changes in surface temperature (°C, contours and shadings) and wind (m/s, arrows) in the summer (June to August – JJA; left) and winter (December to February – DJF; right) following the AOD imposed anomalies for extreme experiments (MC extreme – A and B; and EqPAC extreme – C and D) relative to the no-volcano case. Only temperature values that are significantly different at the 5% level using a local (grid-point) *t* test are shaded. The contours follow the colorbar intervals (solid for positive and dashed for negative anomalies; the zero line is omitted).

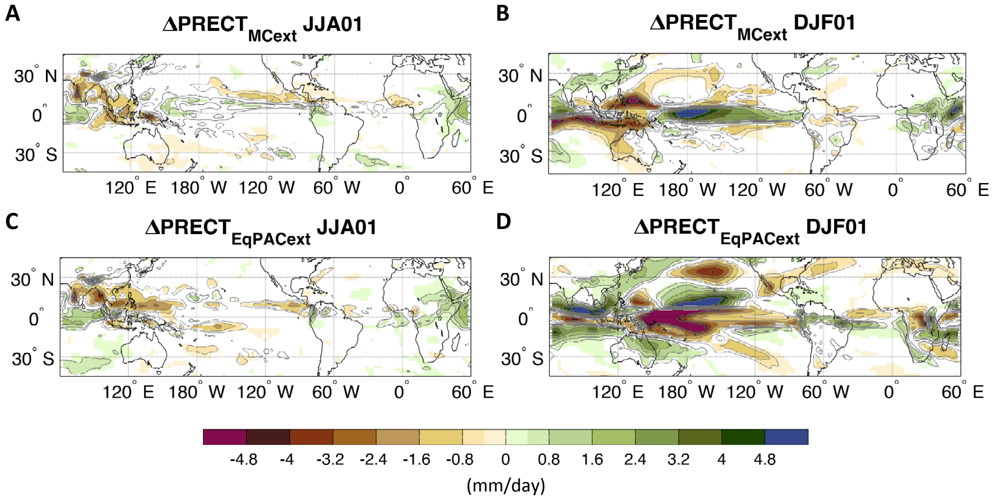

Figure S7. Rainfall response for the extreme experiments. Changes in precipitation (mm/day, contours and shadings) in the summer (June to August – JJA) and winter (December to February – DJF) following the AOD imposed anomalies for extreme experiments (MC extreme – A and B; and EqPAC extreme – C and D) relative to the no-volcano case. Only temperature values that are significantly different at the 5% level using a local (grid-point) *t* test are shaded. The contours follow the colorbar intervals (solid for positive and dashed for negative anomalies; the zero line is omitted).

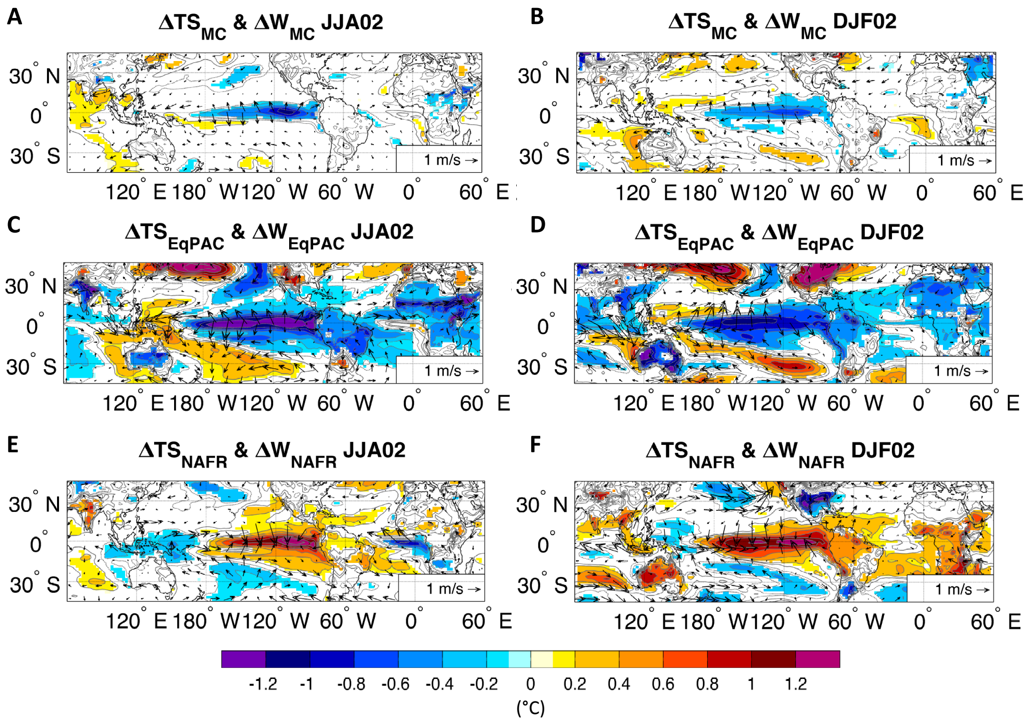

Figure S8. Surface air temperature and wind response in the second post-eruption year. Changes in surface temperature (°C, contours and shadings) and wind (m/s, arrows) in the summer (June to August – JJA) and winter (December to February – DJF) following the AOD imposed anomalies above the Maritime Continent – MC (A and B), the equatorial Pacific – EqPAC (C and D) and the tropical and northern Africa – NAFR (E and F). Only temperature values that are significantly different at the 5% level using a local (grid-point) *t* test are shaded. The contours follow the colorbar intervals (solid for positive and dashed for negative anomalies; the zero line is omitted).